Shape Analysis of Planar Objects with Arbitrary Topologies using Conformal Geometry

Lok Ming Lui, Wei Zeng, Shing-Tung Yau, Xianfeng Gu

Abstract

The study of 2D shapes is a central problem in the field of computer vision. In 2D shape analysis, classification and recognition of objects from their observed silhouette are extremely crucial and yet difficult. It usually involves an efficient representation of 2D shape space with natural metric, so that its mathematical structure can be used for further analysis. Although significant progress has been made for the study of 2D simply-connected shapes, very few works have been done on the study of 2D objects with arbitrary topologies. In this work, we proposed a representation of general 2D domains with arbitrary topologies using conformal geometry. A natural metric can be defined on the proposed representation space, which gives a metric to measure dissimilarities between objects. The main idea is to map the exterior and interior of the domain conformally to unit disks and punctual disks (circle domains), using holomorphic 1-forms. A set of diffeomorphisms from the unit circle $\mathbb{S}^1$ to itself can be obtained, which together with the conformal modules are used to define the shape signature. We prove mathematically that our proposed signature uniquely represents shapes with arbitrary topologies. We also introduce a reconstruction algorithm to obtain shapes from their signatures. This completes our framework and allows us to go back and forth between shapes and signatures. Experimental results shows the efficacy of our proposed algorithm as a stable shape representation scheme.

Index Terms

Shape analysis; conformal geometry; holomorphic 1-form; conformal modules; shape signature.

I. Introduction

Shape analysis of planar objects from their observed silhouette is important for many computer vision applications, such as classification, recognition and image retrieval. In order to perform shape analysis effectively, it is necessary to have an efficient representation of shapes and a robust metric measuring their dissimilarity.

Recently, many different representations for 2D shapes and various measures of dissimilarity between them have been proposed. For example, Zhu et al. [1] proposed the representation of shapes using their medial axis and compare their skeletal graphs through a branch and bound strategy. Liu et al. [2] use shape axis trees to represent shapes, which are defined by the locus of midpoints of optimally corresponding boundary points. Belongie et al. [3] proposed to represent and match 2D shapes for object recognition, based on the shape context and the Hungarian method. Mokhtarian [4] introduced a multi-scale, curvature-based shape representation technique for planar curves, which is especially suitable for recognition of a noisy curve. Besides, various statistical models for shape representation were also proposed by different research groups [5], [6], [7]. These approaches provide a simple way to represent shapes with finite dimensional spaces, although they cannot capture all the variability of shapes. Yang et al. [8] proposed

a signal representation approach called the Schwarz representation and applied it to shape matching problems. Lee et al. [9] proposed to represent curves based on their complete silhouettes, through the use of harmonic embedding. Mumford et al. [10] proposed a conformal approach to model simple closed curves which captured subtle variability of shapes up to scaling and translation. They also introduced a natural metric, called the Weil-Petersson metric, on the proposed representation space.

Most of the above methods work only on simple closed curves and generally cannot deal with multiply-connected objects. In real world applications, objects from their observed silhouette are usually multiply-connected domains (i.e. domains with holes in the interior). For example, the silhouette of a human face with the mouth and eyes is a multiply-connected shape. A lot of images from the real world consists of multiple objects, which are essentially multiply-connected. In order to analyze shapes or images with arbitrary topologies effectively, it is necessary to develop an algorithm which can deal with multiply-connected domains. This motivates us to look for a good representation, which is equipped with a natural metric, to model planar objects of arbitrary topologies.

In this paper, we extended Mumford's conformal approach [10], which models 2D simply-connected domains, to represent multiply-connected shapes. Mumford's approach provides an effective way to represent 2D simple curves and capture their subtle differences. We believe an extension of this approach to multiply-connected shapes is helpful for the purpose of classification and image understanding. The key idea of our method is to map the exterior and interior of the domain conformally to unit disks and punctual disks, using holomorphic 1-forms. A set of diffeomorphisms from the unit circle $\mathbb{S}^1$ to itself can be obtained, which together with the conformal modules are used to define the shape signature. It can be proven that our proposed signature uniquely represents shapes with arbitrary topologies up to scaling and translation. We also introduce a reconstruction algorithm to obtain shapes from their signatures, by solving the Beltrami equation. This completes our framework and allows us to move back and forth between shapes and signatures. The proposed representation space inherits a natural metric that can be used to measure dissimilarity between shapes.

II. Theoretically background

In this section, we briefly introduce the theoretical foundations necessary for the current work. For more details, we refer readers to the classical books [11], [12], [13], [14].

A. Beltrami Equation

Consider a complex valued function $\phi : \mathbb{C} \to \mathbb{C}$ maps the z-plane to the w-plane, where $z = x + iy$, $w = u + iv$. The *complex partial derivative* is defined as:

$$\frac{\partial}{\partial z} := \frac{1}{2}(\frac{\partial}{\partial x} - i\frac{\partial}{\partial y}), \frac{\partial}{\partial \bar{z}} = \frac{1}{2}(\frac{\partial}{\partial x} + i\frac{\partial}{\partial y}) \tag{1}$$

The *Beltrami equation* for ϕ is defined by:

$$\frac{\partial \phi}{\partial \bar{z}} = \mu(z)\frac{\partial \phi}{\partial z} \tag{2}$$

where μ is called the *Beltrami coefficient*.

If μ is zero, then ϕ is called a *holomorphic or conformal mapping*. Otherwise, if $\|\mu\|_\infty < 1$, then ϕ is called a *quasiconformal mapping*. In terms of the metric tensor, consider the effect of the pullback under ϕ of the usual Euclidean metric ds_E^2; the resulting metric is given by:

$$\phi^*(ds_E^2) = |\frac{\partial \phi}{\partial z}|^2 |dz + \mu(z)d\overline{z}|^2. \tag{3}$$

which, relative to the background Euclidean metric dz and $d\overline{z}$, has eigenvalues $(1+|\mu|)^2\frac{\partial f}{\partial z}$ and $(1-|\mu|)^2\frac{\partial f}{\partial z}$. μ is called the *Beltrami coefficient*, which is a measure of non-conformality. In particular, the map ϕ is conformal around a small neighborhood of p when $\mu(p) = 0$. Infinitesimally, around a point p, ϕ may be expressed with respect to its local parameter as follows:

$$\begin{aligned} f(z) &= f(p) + f_z(p)z + f_{\overline{z}}(p)\overline{z} \\ &= f(p) + f_z(p)(z + \mu(p)\overline{z}). \end{aligned} \tag{4}$$

Obviously, f is not conformal if and only if $\mu(p) \neq 0$. Inside the local parameter domain, f may be considered as a map composed of a translation to $f(p)$ together with a stretch map $S(z) = z + \mu(p)\overline{z}$, which is postcomposed by a multiplication of $f_z(p)$, which is conformal. All the conformal distortion of $S(z)$ is caused by $\mu(p)$. $S(z)$ is the map that causes f to map a small circle to a small ellipse. From $\mu(p)$, we can determine the angles of the directions of maximal magnification and shrinking and the amount of them as well. Specifically, the angle of maximal magnification is $\arg(\mu(p))/2$ with magnifying factor $1 + |\mu(p)|$; The angle of maximal shrinking is the orthogonal angle $(\arg(\mu(p)) - \pi)/2$ with shrinking factor $1 - |\mu(p)|$. The distortion or dilation is given by:

$$K = (1 + |\mu(p)|)/(1 - |\mu(p)|). \tag{5}$$

Thus, the Beltrami coefficient μ gives us important information about the properties of the map (See Figure 1).

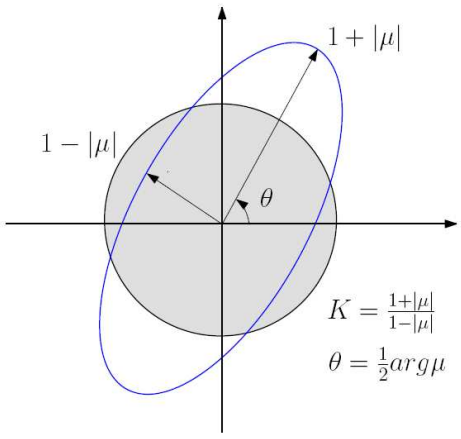

Fig. 1. Illustration of how the Beltrami coefficient μ measures the distortion of a quasi-conformal mapping that maps a small circle to an ellipse with dilation K.

Given a compact simply-connected domain Ω in $\mathbb{C}$ and a Beltrami coefficient μ with $\|\mu\|_\infty < 1$. There is always a quasiconformal mapping from Ω to the unit disk $\mathbb{D}$ which satisfies the Beltrami equation in the distribution sense [11]. More precisely,

Theorem *2.1 (Measurable Riemann Mapping Theorem):* Suppose Ω is a simply connected domain in $\mathbb{C}$ that is not equal to $\mathbb{C}$, and suppose that $\mu : \Omega \to \mathbb{C}$ is Lebesgue measurable and satisfies $\|\mu\|_\infty < 1$, then there is a quasiconformal hoemorphism ϕ from Ω to the unit disk, which is in the Sobolev space $W^{1,2}(\Omega)$ and satisied the Beltrami equation 2 in the distribution sense.

This theorem plays a fundamental role in this work. Suppose $f, g : \mathbb{C} \to \mathbb{C}$ are with Beltrami coefficients μ_f, μ_g respectively. Then the Beltrami ceofficient for the composition $\phi_2 \circ \phi_1$ is given by

$$\mu_{g\circ f} = \frac{\mu_f + (\mu_g \circ f)\tau}{1 + \bar{\mu_f}(\mu_g \circ f)\tau} \tag{6}$$

where $\tau = \frac{\bar{f_z}}{f_z}$.

B. Conformal Module

Suppose Ω_1 and Ω_2 are planar domains. We say Ω_1 and Ω_2 are *conformally equivalent* if there is a biholomorphic diffeomorphism between them. All planar domains can be classified by the conformal equivalence relation. Each conformal equivalence class shares the same *conformal invariants*, the so-called *conformal module*. The conformal module is one of the key component for us to define the unique shape signature.

Suppose Ω is a compact domain on the complex plane $\mathbb{C}$. If Ω has a single boundary component, the it is called a *simply connected domain*. Every simply connected domain can be mapped to the unit disk conformally and all such kind of mappings differ by a *Möbius transformation*: $z \to e^{i\theta}\frac{z-z_0}{1-\bar{z}_0 z}$.

Suppose Ω has multiple boundary components $\partial\Omega = \gamma_0 - \gamma_1 - \gamma_2 \cdots \gamma_n$, where γ_0 represent the exterior boundary component, then Ω is called a *multiply-connected planar domain*. A *circle domain* is a unit disk with circular holes. Two circle domains are conformally equivalent, if and only if they differ by a Möbius transformation. It turns out every multiply-connected domain can be conformally mapped to a circle domain, as described in the following theorem.

Theorem *2.2 (Riemann Mapping for Multiply Connected Domain):* If Ω is a multiply-connected domain, then there exists a conformal mapping $\phi : \Omega \to D$, where D is a circle domain. Such kind of mappings differ by Möbius transformations.

Therefore, each multiply connected domain is conformally equivalent to a circle domain. The conformal module for a circle domain is represented as the centers and radii of inner boundary circles. All simply-connected domains are conformally equivalent. The topological annulus requires 1 parameter to represent the conformal module. In general case, because there are $n > 1$ inner circles, and the Mobius transformation group is 3 dimensional, therefore the conformal module requires $3n - 3$ parameters. We denote the conformal module of Ω as $Mod(\Omega)$.

Fix n, all conformal equivalence classes form a $3n-3$ Riemannian manifold, the *Teichmüller space*. The conformal module can be treated as the Teichmüller coordinates. The Weil-Peterson metric [10] is a Riemannian metric for Teichmüller space, which induces negative sectional curvature, therefore, the geodesic between arbitrary two points is unique.

C. Holomorphic Differentials

In order to compute the conformal modules, one needs to find the holomorphic differential forms on the multiply connected domain. A *differential 1-form* on a planar domain ω is defined as

$$\tau = f(x,y)dx + g(x,y)dy,$$

where f, g are smooth functions. A *harmonic 1-form* is curl free and divergence free

$$\nabla \times \tau = 0, \nabla \cdot \tau = 0,$$

where the differential operator $\nabla = (\frac{\partial}{\partial x}, \frac{\partial}{\partial y})$. If τ is the gradient of another function defined on Ω, then it is called an *exact 1-form*.

The *Hodge star* operator acting on a differential 1-form gives the *conjugate differential 1-form*

$$^*\tau = -g(x,y)dx + f(x,y)dy,$$

intuitively, the conjugate 1-form $*\tau$ is obtained by rotating τ by a right angle everywhere. If τ is harmonic, so is its conjugate $*\tau$.

A *holomorphic 1-form* consists of a pair of conjugate harmonic 1-forms

$$\omega = \tau + i\ ^*\tau = \phi(z)dz,$$

where $\phi(z)$ is a holomorphic function. We further requires that either τ or $^*\tau$ is orthogonal to all the boundaries. All the holomorphic 1-forms consist a group (with real coefficients), denoted as $\mathbb{H}(\Omega)$. A basis of $\mathbb{H}(\Omega)$ is given by

$$\{\omega_1, \omega_2, \cdots, \omega_n\},$$

such that $\int_{\gamma_j} \omega_i = \delta_i^j$, where δ_i^j is the Kronecker symbol. By using the holomorphic 1-forms, one can construct the following *circular slit map*.

Theorem *2.3 (Circular Slit Map):* Suppose a multiply connected domain Ω with more than one boundary components, then there exists a conformal mapping $\phi : \Omega \to \mathbb{C}$, such that γ_0, γ_1 are mapped to concentric circles, γ_k's are mapped to concentric circular slits. All such kind of mappings differs by a rotation.

D. Conformal Welding

This work is built on *conformal welding*, which is constructed as follows. Suppose $\Gamma = \{\gamma_0, \gamma_1, \cdots, \gamma_k\}$ are non-intersecting smooth closed curves on the complex plane. Γ segments the plane to a set of connected components $\{\Omega_0, \Omega_1, \cdots, \Omega_s\}$, each segment Ω_i is a multiply-connected domain. We assume Ω_0 contains the infinity point, $p \notin \Omega_0$. By using a Möbius transformation $\phi(z) = \frac{1}{z-p}$, p is mapped to ∞, Ω_0 is mapped to a compact domain. Replace Ω_0 by $\phi(\Omega_0)$. Construct $\phi_k : \Omega_k \to \mathbb{D}_k$ to map each segment Ω_k to a circle domain $\mathbb{D}_k$, $0 \leq k \leq s$. Assume $\gamma_i \in \Gamma = \Omega_j \cap \Omega_k$, then $\phi_j(\gamma_i)$ is a circular boundary on the circle domain $\mathbb{D}_j$, $\phi_k(\gamma_i)$ is a another circle on $\mathbb{D}_k$. Let $f_i = \phi_j \circ \phi_k^{-1} : \mathbb{S}^1 \to \mathbb{S}^1$ be the diffeomorphism from the circle to itself, which is called the *signature of* γ_i.

Definition *2.4 (Signature of a family of loops):* The signature of a family non-intersecting closed planar curves $\Gamma = \{\gamma_0, \gamma_1, \cdots, \gamma_k\}$ is defined as

$$S(\Gamma) := \{f_0, f_1, \cdots, f_k\} \cup \{Mod(\mathbb{D}_0), Mod(\mathbb{D}_1), \cdots, Mod(\mathbb{D}_s)\}.$$

The following main theorem plays the fundamental role for the current work.

Theorem *2.5 (Main Theorem):* The family of smooth planar closed curves Γ is determined by its signature $S(\Gamma)$, unique up to a Möbius transformation of the Riemann sphere $\mathbb{C} \cup \{\infty\}$.

Note that if a circle domain $\mathbb{D}_k$ is disk, its conformal module can be omitted from the signature. The Möbius transformation of the Riemann sphere is given by $(az+b)/(cz+d)$, where $ad-bc = 1, a, b, c, d \in \mathbb{C}$. The proof of Theorem 2.5 can be found in the Appendix.

The theorem states that the proposed signature determine shapes up to a Möbius transformation. We can further do a normalization that fixes ∞ to ∞ and that the differential carries the real positive axis at ∞ to the real positive axis at ∞, as in Mumford's paper [10]. The signature can then determine the shapes uniquely up to translation and scaling.

The shape signature $S(\Gamma)$ gives us a complete representation for the space of shapes. It inherits a natural metric. Given two shapes Γ_1 and Γ_2. Let $S(\Gamma_i) := \{f_0^i, f_1^i, \cdots, f_k^i\} \cup \{Mod(\mathbb{D}_0^i), Mod(\mathbb{D}_1^i), \cdots, Mod(\mathbb{D}_s^i)\}$ ($i = 1, 2$). We can define a metric $d(S(\Gamma_1), S(\Gamma_2))$ between the two shape signatures using the natural metric in the Teichmuller space, such as the Weil-Petersson metric [10].

III. Algorithm

In this section, we describe in detail the algorithm to compute the signature of a planar domain and the algorithm to reconstruct the shapes from their signatures.

Here, we assume a planar domain Ω is with n inner boundary components, Let the boundary of the mesh is $\partial\Omega = \gamma_0 - \gamma_1 \cdots - \gamma_n$, represented as a triangular mesh. We use v_i to denote a vertex, $[v_i, v_j]$ denote an edge, $[v_i, v_j, v_k]$ denote face. We define the angle structure of the mesh as:

Definition *3.1 (Angle Structure):* The angle at vertex v_i in triangle $[v_i, v_j, v_k]$ is denoted as θ_{jk}^i. The corner angle of the mesh is defined as the set

$$A(\Omega) := \{\theta_{jk}^i, \theta_{ij}^k, \theta_{ki}^j | [v_i, v_j, v_k] \in \Omega\}.$$

All the following computations completely depend on the angle structure.

A. Discrete Holomorphic 1-Form

In this work, holomorphic 1-forms are used to compute the conformal parameterizations of the planar object to circle domains. The conformal parameterization computed is then used to compute the shape signature of the object. In this subsection, we will explain how the discrete holomorphic 1-form can be computed.

Discrete Differential Operators: The discrete functions defined on vertices, edges and faces are called discrete 0-forms, 1-forms and 2-forms respectively.

The gradient of a 0-form f, df is a discrete 1-form, which is given by

$$df([v_i, v_j]) = f(v_j) - f(v_i).$$

The *curl* of a discrete 1-form ω is given by

$$curl\ \omega([v_i, v_j, v_k]) = \omega(\partial[v_i, v_j, v_k]) = \omega([v_i, v_j]) + \omega([v_j, v_k]) + \omega([v_k, v_i]).$$

The *div* of ω is given by

$$div\ \omega(v_i) = \sum_{[v_i, v_j] \in \Omega} w_{ij}\ \omega([v_i, v_j]),$$

where w_{ij} is the *edge weight*, defined as the follows:

$$w_{ij} := \begin{cases} \cot \theta_{ij}^k + \cot \theta_{ji}^l & [v_i, v_j] \notin \partial\Omega \\ \cot \theta_{ij}^k & [v_i, v_j] \in \partial\Omega \end{cases}$$

where θ_{ij}^k and θ_{ij}^l are the corner angles on the faces adjacent to the edge $[v_i, v_j]$ and against the edge.

The *discrete wedge operator* $\wedge$ is defined as following. Given $[v_i, v_j, v_k] \in \Omega$, τ_1, τ_2 are discrete 1-forms, then

$$\tau_1 \wedge \tau_2([v_i, v_j, v_k]) = \frac{1}{2} \begin{vmatrix} \tau_1([v_i, v_j]) & \tau_2([v_i, v_j]) \\ \tau_1([v_j, v_k]) & \tau_2([v_j, v_k]) \end{vmatrix}.$$

Discrete Harmonic Functions: Let f be a discrete function. We say f is a discrete harmonic function, if it satisfies the following equation:

$$div\ df(v_i) = 0, \forall v_i \notin \partial\Omega.$$

We compute n harmonic functions, $f_k : \Omega \to \mathbb{R}, k > 0$, which satisfies the above equation with the boundary condition

$$f_k(v_i) = 1, \forall v_i \in \gamma_k, f_k(v_j) = 0, \forall v_j \in \partial\Omega, \notin \gamma_k.$$

Let $\tau_k = df_k, 1 \leq k \leq n$, then $\{\tau_1, \tau_2, \cdots, \tau_n\}$ form the basis for all exact harmonic 1-forms on Ω.

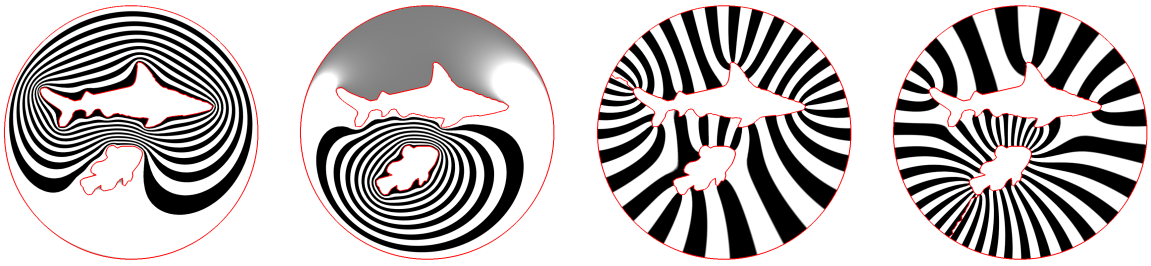

(a) Exact form τ_1 (b) Exact 1-form τ_2 (c) Closed form τ_3 (d) Closed form τ_4

Fig. 2. Harmonic 1-form basis.

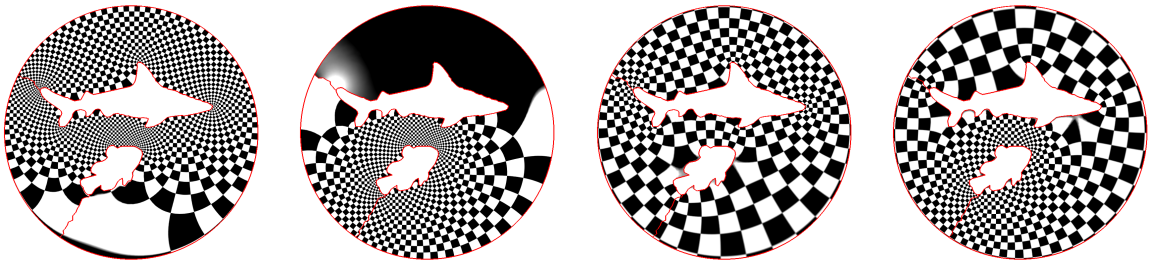

Fig. 3. Holomorphic 1-form basis $\{\omega_1, \omega_2, \omega_3, \omega_4\}$.

Discrete Harmonic 1-forms: We compute the shortest cut η_k from γ_k to γ_0, $1 \leq k \leq n$. Then we slice Ω along η_k to get an $\tilde{\Omega}_k$, such that the shortest path η_k becomes η_k^+ and η_k^-. Then we construct a function $h_k : \tilde{\Omega}_k \to \mathbb{R}$, such that

$$h_k(p) = 1, \forall p \in \eta_k^+; \quad h_k(p) = 0, \forall p \in \eta_k^-;$$

and $h_k(p)$ is random for all interior vertices on $\tilde{\Omega}_k$. Then dh_k is a *discrete exact 1-form* on $\tilde{\Omega}_k$. Because of the consistency along the boundaries, dh_k is also a closed 1-form (but not exact) on Ω. We compute a function g_k such that $dh_k + dg_k$ is a harmonic 1-form by solving the equation,

$$div(dh_k + dg_k)(v_i) = 0, \forall v_i \notin \partial\Omega.$$

Let $\tau_{n+k} := dh_k + dg_k, 1 \leq k \leq n$, the $\{\tau_{n+1}, \tau_{n+2}, \cdots, \tau_{2n}\}$ form the basis for all closed (non-exact) harmonic 1-form group on Ω (See Figure 2).

Holomorphic Differential: A holomorphic 1-form can be constructed by a harmonic 1-form and its conjugate $\tau_k + i^*\tau_k$, where * is the Hodge star operator. The conjugate form of a harmonic 1-form is still a harmonic 1-form. Therefore,

$$^*\tau_k = \sum_{i=1}^{2n} c_{ki}\tau_i,$$

where c_{ki}'s are unknown real numbers. By solving the following linear system

$$\int_\Omega \tau_j \wedge {}^*\tau_k = \sum_{i=1}^{2n} c_{ki} \int_\Omega \tau_j \wedge \tau_i, j = 1, 2, \cdots, 2n, \tag{7}$$

we can find all the unknowns and get the conjugate form. Let ω_k denote $\tau_k + i^*\tau_k$, then

$$\{\omega_1, \omega_2, \cdots, \omega_{2n}\}$$

form a basis for holomorphic 1-form group of the surface.

The *discrete Hodge Star* * is defined as follows. Each face is a Euclidean triangle embedded on $\mathbb{R}^2$ with the isometric local coordinates (x, y). Suppose τ is a discrete closed 1-form, then it has local representation $\omega = c_1 dx + c_2 dy$, where c_1, c_2 are constants on each face, $^*\omega = c_1 dy - c_2 dx$. Let ω, τ be two discrete harmonic 1-forms, locally $\omega = c_1 dx + c_2 dy$ and $\tau = d_1 dx + d_2 dy$, then locally

$$\omega \wedge {}^*\tau = \begin{vmatrix} c_1 & c_2 \\ d_1 & d_2 \end{vmatrix} dx \wedge dy,$$

Then we can treat $\omega \wedge {}^*\tau$ as a discrete 2-form, such that $\omega \wedge {}^*\tau([v_i, v_j, v_k]) = (c_1 d_2 - c_2 d_1) A_{ijk}$, where A_{ijk} is the area of $[v_i, v_j, v_k]$, then the left hand side of Equation 7 is

$$\int_\Sigma \omega \wedge {}^*\tau = \sum_{[v_i, v_j, v_k] \in \Sigma} \omega \wedge {}^*\tau([v_i, v_j, v_k]).$$

Figure 3 shows the holomorphic 1-form group basis for the 2-hole planar domain.

B. Shape signatures of planar domains with arbitrary topologies

We describe the algorithm to compute the signature of Ω with n inner boundary components. The inner boundaries decompose Ω into several sub-domains Ω_k. The algorithm consists of 2 main steps:

Step 1: Compute the conformal maps from Ω_k to circle domains D_k;

Step 2: Compute the conformal modules for each sub-domain Ω_k and the signature f_{ij} for each boundary.

Step 1*: Conformal maps from Ω_k to circle domains D_k:*

The conformal parameterization of Ω_k can be obtained easily by computing the circular slit map and performing the Koebe's iteration. For detail, please refer to [15].

Circular slit:: The circular slit map can be obtained by finding a holomorphic 1-form ω, such that

$$Img(\int_{\gamma_0} \omega) = 2\pi, Img(\int_{\gamma_1} \omega) = -2\pi, img(\int_{\gamma_k} \omega) = 0, 2 \leq k \leq n-1. \tag{8}$$

To solve Equation 8, we first compute the basis for the holomorphic 1-form group. ω is then a linear combination of the basis $\omega = \sum_{k=1}^{n} \lambda_k \omega_k$, the coefficients $\{\lambda_k\}$ can be calculated by solving the linear system 8. The circular slit map is given by $\phi(p) = exp(\int_q^p \omega), \forall p \in \Omega$, where q is a base point, and the integration path is arbitrarily chosen in Ω. Figure 4 shows the circular slit map of a 2-hole planar domain.

If Ω is a simply connected domain (topological disk), we compute the conformal mapping to map it to the unit disk in the following way. First, we punch a small hole in the domain, then treat it as topological annulus. Then we use circular slit map to map the punched annulus to the canonical annulus. By shrinking the size of the punched hole, the circular slit mappings converge to the conformal mapping. Figure 5 shows one such an example.

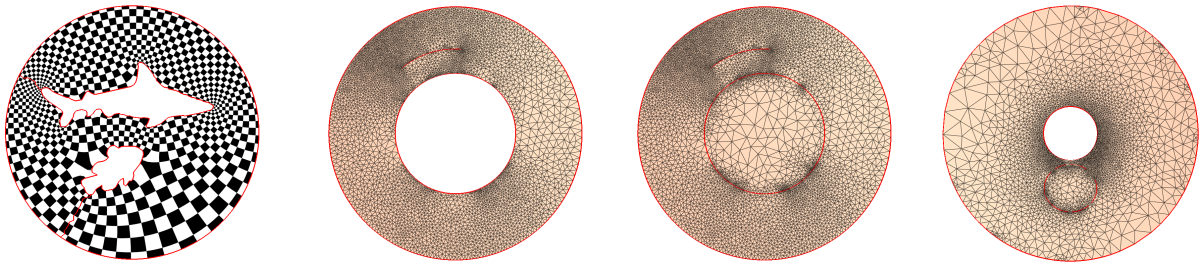

(a) Holomorphic 1-form (b) Circular slit map (c) Fill the inner hole (d) Slit Map of (c)

Fig. 4. Circular slit maps.

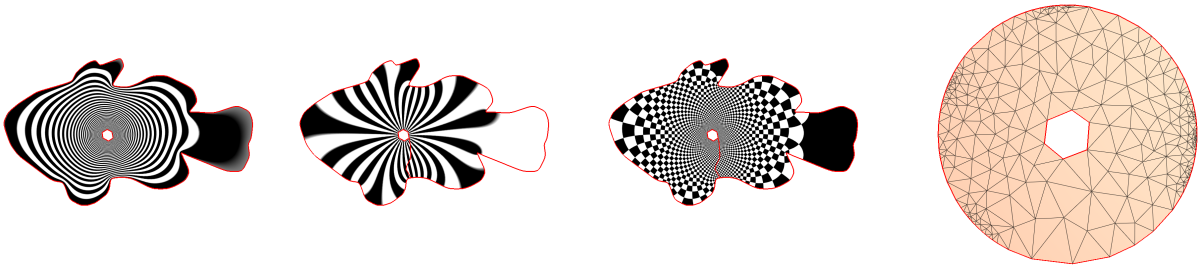

(a) Exact form (b) Closed form (c) Holomorphic form (d) Conformal mapping

Fig. 5. Conformal mapping for a simply connected domain by puncturing a small hole in the center.

Hole Filling:: After computing the circular slit map, the planar domain is mapped to the planar annulus with concentric circular slits. γ_0 is the unit circle, γ_1 is the inner circle, γ_k's are slits. We use Delaunay triangulation to generate a disk D_1 bounded by γ_1, $\partial D_1 = \gamma_1$, and glue Ω with D_1 along γ_1, $\Omega_1 := \Omega \cup_{\gamma_1} D_1$.

We then use circular slit map again to map Ω_1, such that γ_2 is opened to a circle. We compute a disk D_2 bounded by γ_2, glue Ω_1 and D_2 to get Ω_2. By repeating circular slit map, at the step k, γ_k is opened to a circle. We compute a circular disk D_k bounded by γ_k, and glue Ω_{k-1} with D_k, $\Omega_k = \Omega_{k-1} \cup_{\gamma_k} D_k$.

Eventually, we can fill all the holes to get Ω_n. All the disks D_k in Ω_n are not exact circular.

Koebe's iteration:: By Koebe's iteration, all the boundary components become rounder and rounder. Basically, each time, we choose a disk D_k, the complement of D_k on Ω_n is a double connected domain. We map the complement to the canonical planar annulus, then γ_k becomes a circle. We recompute the disk D_k bounded by the updated γ_k, glue the annulus with the updated D_k. After this iteration, γ_k becomes a circle. Then we choose another disk D_j, and repeat this process to make γ_j a circle. This will destroy the perfectness of the circular shape of γ_k. But by repeating this process, all the γ_k's become rounder and rounder, and eventually converge to perfect circles. The convergence is exponentially fast. Detailed proof can be found in [12].

Step 2*: Computing conformal modules and signatures f_{ij} on boundaries:* After the conformal parameterization of Ω_k to the circle domain is computed, we can then compute their conformal modules and also the signature f_{ij} on each boundary. The conformal modules together with $\{f_{ij}\}$ give the complete signature $S(\Gamma)$. We demonstrate the process for computing $S(\Gamma)$ with a double fish image as shown in

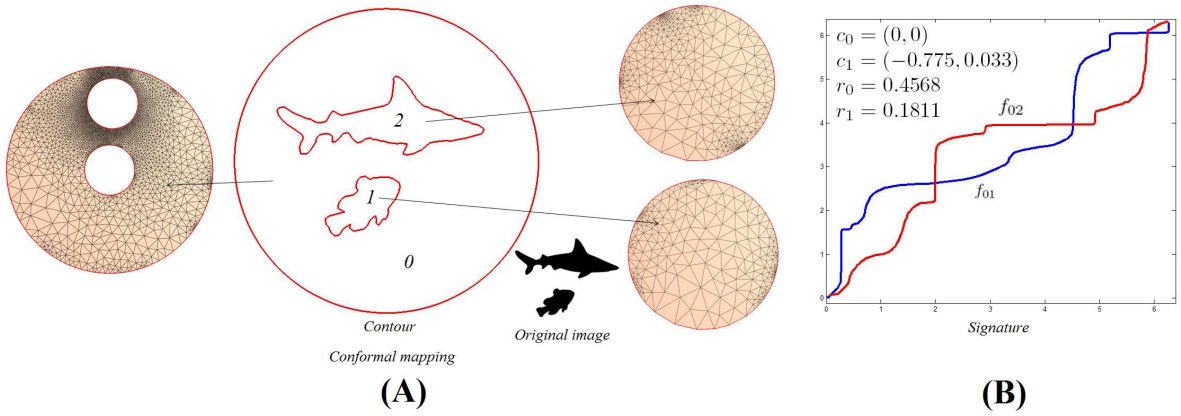

Fig. 6. Signature. Each segment is mapped to a circle domain. The conformal module (centers and radii of inner circles) of the circle domains and the diffeomorphisms of the circles define the signature.

Figure 6. Given the original image, we first perform image segmentation to get the binary image, then calculate the contours of the objects in the image. The contour of each fish is shown in the figure. For simplicity, we treat the outermost boundary of the image as the unit circle. Then all the contours segment the image to planar domains $\Omega_0, \Omega_1, \Omega_2$. We map each planar segment to a circle domain. Ω_0 is mapped to a disk D_0 with two circular holes. The centers and radii (c_0, r_0) and (c_1, r_1) form the conformal module of Ω_0. Also, Ω_1 and Ω_2 are mapped to the unit disks D_1, D_2 respectively. We denote the conformal maps of Ω_i by $\Phi_i : \Omega_i \to D_i$. The contour of the small fish are mapped to the boundary of D_1 and one inner boundary of D_0, the signature is given by $f_{01} := \Phi_1 \circ \Phi_0^{-1}$, which is shown in frame (B) as the blue curve. Similarly, the signature f_{02} of the contour of the shark can also be computed. The signature of both fish contours is given by $S(\Gamma) = \{c_0, c_1, r_0, r_1, f_{01}, f_{02}\}$.

C. Reconstruction of shapes from signatures

The reconstruction of the contours from the signature is straightforward. Suppose there are n contours, then there are $n+1$ segments. The signature is given by the conformal modules $\{Mod(D_k), 0 \leq k \leq n\}$ and automorphims of circles f_{ij}.

First, we construct circle domains D_k's directly from their modules $Mod(D_k)$'s. Each we tessellate the circular boundaries of each D_k and use Delaunay triangulation to triangulate D_k. Then, we combinatorially glue the triangle mesh D_i and D_j by f_{ij}. Suppose the boundary circle $\gamma_i \in \partial D_i$ corresponds to $\gamma_j \in D_j$, $f_{ij} : \gamma_i \to \gamma_j$. For each vertex $v_i \in \gamma_i$, we insert $f_{ij}(v_i)$ to γ_j, vice versa, for each vertex $v_j \in \gamma_j$, we insert $f_{ij}^{-1}(v_j)$ to γ_i. Then we use constrained Delaunay triangulation to refine the triangulation of D_i and D_j. Therefore the refined triangle mesh D_i and D_j can be combinatorially glued through γ_i and γ_j. We repeat this process for all f_{ij}'s, to obtain a combinatorial triangle mesh, denoted as D.

In the whole algorithm pipeline, all the computations solely depends on the angle structure. We define the angle structure of D as

$$A(D) = \cup_{k=0}^{n} A(D_k).$$

Then we compute a conformal mapping ϕ from D to the unit disk using the angle structure $A(D)$. The image $\phi(D)$ differs from the original image by a Möbius transformation. This can be further removed by specifying three vertices on the outer boundary circle.

Suppose in the original image, the positions of three boundary vertices $\{v_0, v_1, v_2\}$ are $\{w_0, w_1, w_2\}$, and their positions in $\phi(D)$ are $\{z_0, z_1, z_2\}$. We need compute a unique Möbius transformation ρ, such that $\rho(z_k) = w_k$. First, we maps the unit disk to the upper half plane by $h(z) = \frac{z-i}{iz-1}$. Then on the upper half plane, we map $\{h(z_0), h(z_1), h(z_2)\}$ to $\{0, 1, \infty\}$ by

$$\sigma_1(z) = \frac{z - h(z_0)}{z - h(z_2)} \frac{h(z_1) - h(z_2)}{h(z_1) - h(z_0)}.$$

Similarly, we construct $\sigma_2(z)$, that maps $\{h(w_0), h(w_1), h(w_2)\}$ to $\{0, 1, \infty\}$. The the composition map $\sigma = h^{-1} \circ \sigma_2^{-1} \circ \sigma_1 \circ h$ is the desired Möbius transformation, which is called *normalization map*. Therefore, $\tau \circ \phi$ maps D to the unit disk, which reconstructs the contours from the signature.

IV. Experimental results

In this section, we present the experimental results which demonstrate the effectiveness of our proposed shape representation framework for multiply-connected objects. The test data used for experiments are real images obtained from the world wide web. We implement our algorithm using generic C++ on windows XP platform, with Intel Duo CPU 2.33 GHz, 3.98 G RAM. The numerical systems are solved using Matlab C++ library. The contour extraction is obtained by using the OpenCV library. The computational time for our algorithm is as shown in Table II. In general, both the signature calculation and reconstruction take less than 1 minute to compute, even on complicated domains.

A. Shape representation of multiply-connected domains

We tested our method on different real images to demonstrate the effectiveness of our algorithm. Figure 7(A) shows another double fishes image with spatial changes in the positions of the two fishes, compared with that in Figure 6. The big shark and small fish interchanged their positions. The shape signature of the image is plotted in (B), which is quite different from the shape signature in Figure 6 (see red and blue curves). In other words, our shape signature can effectively capture spatial changes of objects in the image, which can be used for the purpose of image understanding.

Figure 8 shows the shape signatures of 3 different images with 3 boundaries and 2 levels. (A) shows the shape signature of the flower image. Note that the fluctuating pattern of the outer boundary of the flower is effectively captured by f_{01} (the red curve). (B) and (C) shows the shape signatures of the brain and elephant images respectively. The three different images have very different shape signatures, meaning that our shape representation can effectively be used for classifying shapes.

We also computed the shape signatures on more complicated images. Figure 10 shows a wolf image with 3 boundaries and 1 level. The exterior and interior of the domain are conformally mapped to the unit disk and punctual disk. The conformal domains consist of one punctual disk with 3 inner disks removed. So, the conformal modules consists of 3 centers and 3 radii, as shown in (B). The diffeomorphisms of

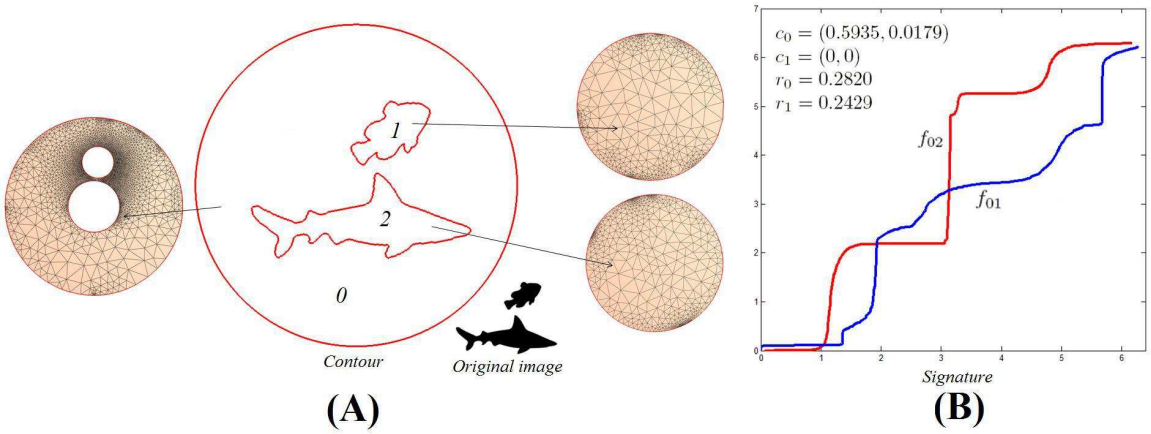

Fig. 7. The shark image with spatial changes in the positions of the two fishes. The shape signature can effectively capture spatial changes of objects in the image (compared to Figure 6).

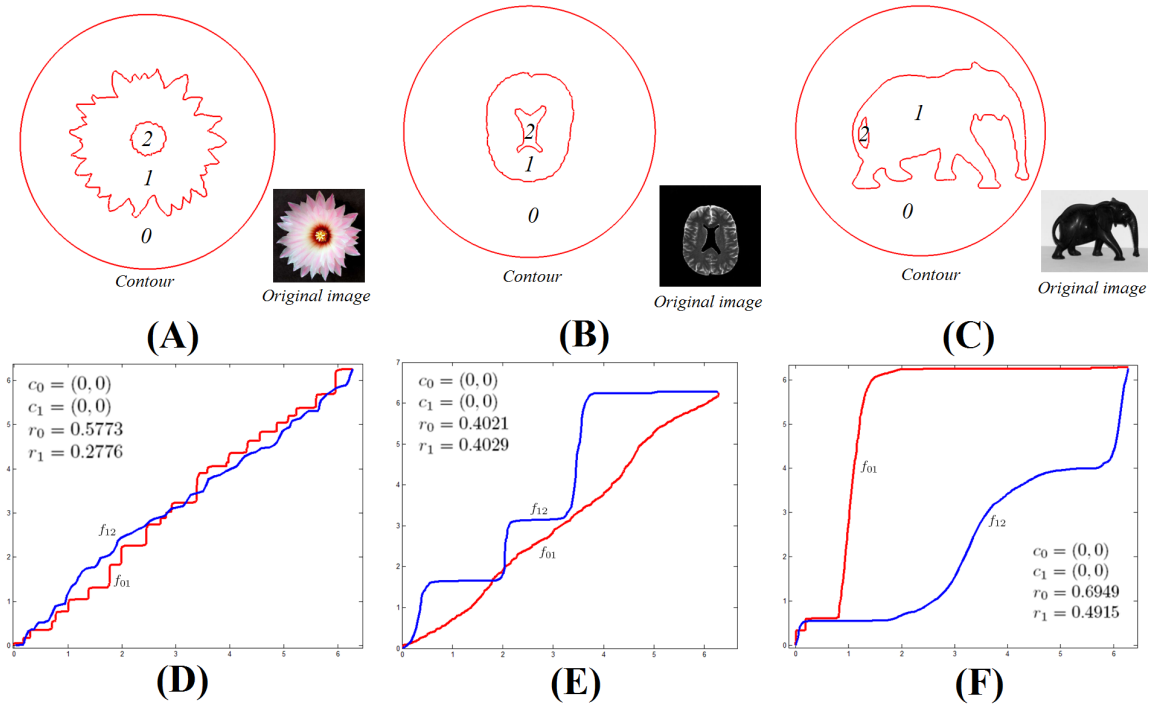

Fig. 8. Shape signatures of different images with 2 boundaries and 2 levels.

the unit circle on each boundary are also plotted in (B). (C) shows the shape signature of the Mickey Mouse image with 3 boundaries and 2 levels. The conformal domain consists of two punctual disks. So, the conformal modules again consist of 3 centers and radii. The conformal modules together with the diffeomorphisms of the unit circle are plotted in (D). Figure 10 shows an image with two cats. It consists of 6 boundaries with 2 levels. The conformal modules consists of 3 punctual disks with 3 holes removed. Hence, the conformal modules consists of 6 centers and 6 radii. The shape signatures are plotted in (B) and (C). (B) shows the signature for the outer level whereas (C) shows the signature of the inner level. Experimental results on these complicated images demonstrate the efficacy of our shape representation method.

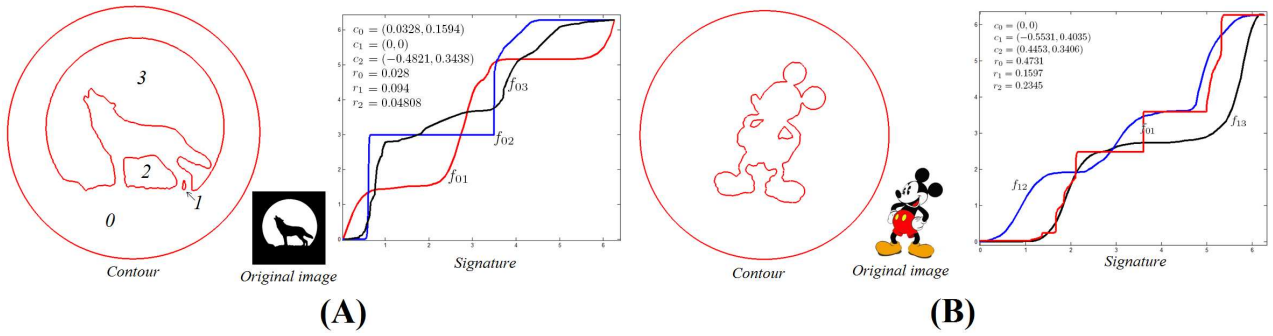

Fig. 9. Shape signatures of different images with 3 boundaries and 2 levels.

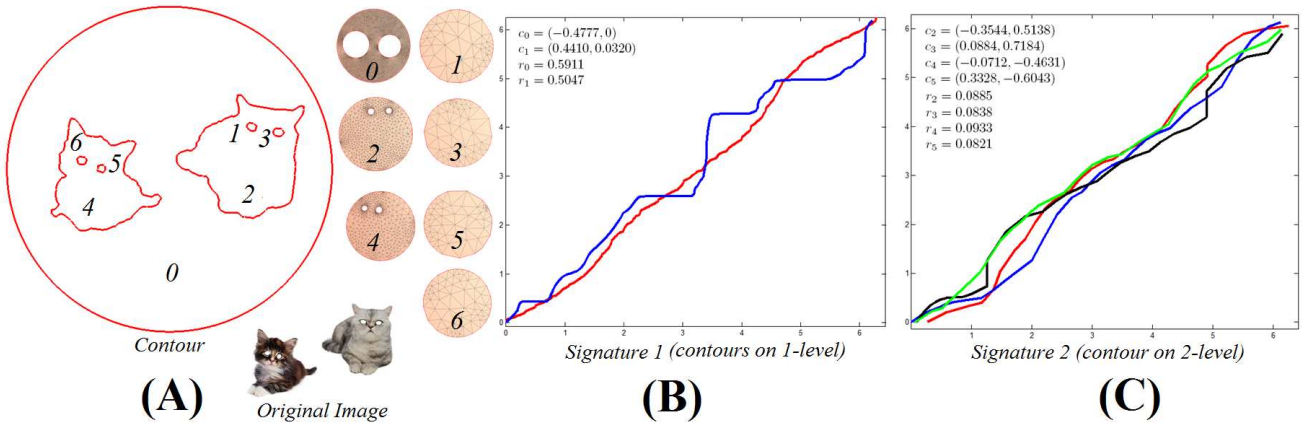

Fig. 10. Shape signatures of another image of cats with 6 boundaries and 2 levels.

B. Reconstruction of shapes from their shape signatures

We also tested our proposed algorithm to reconstruct shapes from their signatures. Figure 11 shows the reconstruction of the shark image from its shape signature. The reconstructed image closely resemble to the original image, except some very tiny details are missing. The zoomed views show that the reconstructed ones are smoother, and lose the sharp corners. It shows our algorithm can effectively reconstruct shapes from their signature.

We also tested our reconstruction algorithm on images with 2 levels. Figure 12 shows the Ameba image with 2 boundaries and 2 levels. The conformal domains consist of two punctual disks, each has one hole removed. The conformal modules consist of two centers and two radii. The shape signature is plotted in (B). We reconstruct the image from its shape signature in (C), which is very close to the original image. We also tested the algorithm on a more complicated example. Figure 13 shows a cat image with 3 boundaries and 2 levels. As we can see in (A), the original contour of the image is a little bit noisy. We computed the shape signature of the image, which is shown in (B). In (C), we show the reconstructed image from its shape signature. Again, the reconstructed image is very close to the original one, although the original noisy contours are smoothed out a little bit.

Finally, we studied the numerical error of our reconstruction scheme. Table I shows the distance between the original and reconstructed contours of the Ameba and cat images. It shows a very small numerical

TABLE I

DISTANCE BETWEEN THE ORIGINAL AND RECONSTRUCTED CONTOURS

Ameba	Number of vertex	Distance sum	Average distance
Contour 1	685	1.669626	0.002437
Contour 2	112	0.238269	0.002127
Cat	Number of vertex	Distance sum	Average distance
Contour 1	96	0.227687	0.002372
Contour 2	92	0.295533	0.003212
Contour 3	363	1.674350	0.004613

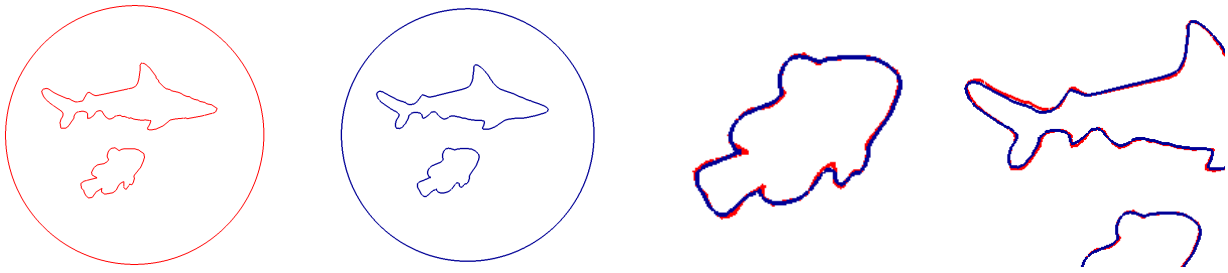

(a) Original contour (b) Reconstructed contour (c) Zoomed view (d) Zoomed view

Fig. 11. Comparison between the original contours (a) and the reconstructed ones (b). The zoomed views (c) and (d) show that the reconstructed ones are smoother.

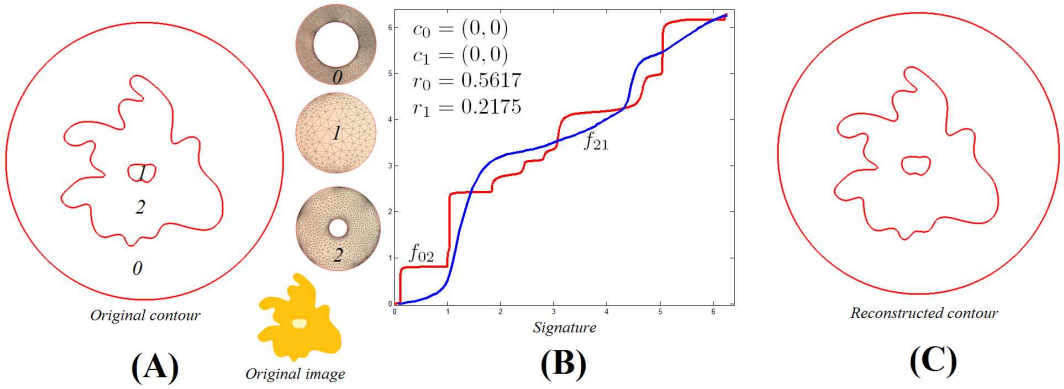

Fig. 12. Shape representation of the Ameba image and the reconstruction from its shape signature.

error. The average distance is less than 0.005. It means our proposed reconstruction algorithm is very accurate.

V. CONCLUSION AND FUTURE WORK

In this paper, we present a shape representation of multiply-connected planar domains using conformal geometry. The main idea is to map the exterior and interior of the domain conformally to unit disks and punctual disks (circle domains). A set of diffeomorphisms from the unit circle $\mathbb{S}^1$ to itself can be obtained, which together with the conformal modules are used to define the shape signature. We also introduce a reconstruction algorithm to obtain shapes from their signatures. This completes the framework of our

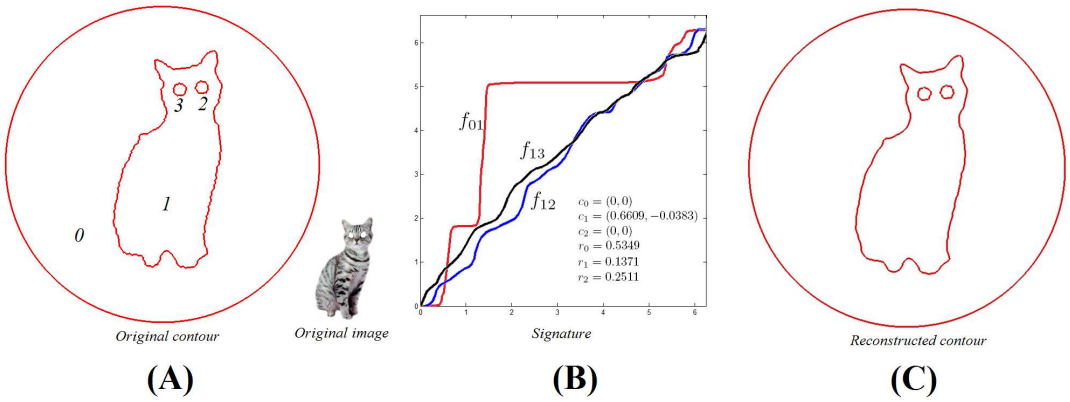

Fig. 13. Shape representation of the cat image and its reconstruction from the shape signature.

TABLE II

COMPUTATIONAL TIME

Model	# of contours	# of vertex	# of faces	Signature	Reconstruction
cat	3	5247	10236	19 Secs	10 Secs
2cats	6	5969	11680	29 Secs	7 Sec
Ameba	2	9094	17930	8 Secs	12 Secs
Fishes	2	5978	11716	23 Secs	8 Secs
New Fishes	2	7519	14780	24 Secs	9 Secs
elephant	2	11968	23678	17 Secs	
flower	2	7101	13944	10 Secs	
Mickey	3	7557	14854	16 Secs	
Brain	2	8211	16164	11 Secs	
Wolf	3	8451	16644	47 Secs	

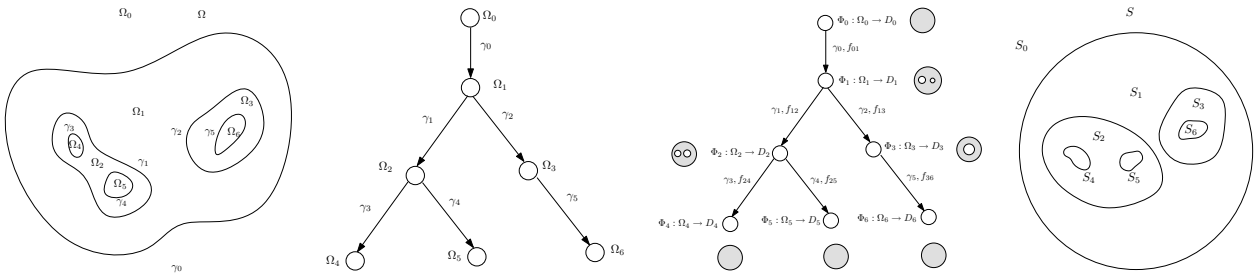

Fig. 14. Proof for the main theorem, the signature uniquely determine the family of closed curves unique up to a Mb̈oius transformation.

shape representation scheme. In the future, we will apply our algorithm for shape analysis based on Weil-Peterson metric.

APPENDIX

Theorem *5.1 (Main Theorem):* The family of smooth planar closed curves Γ is determined by its signature $S(\Gamma)$, unique up to a Möbius transformation of the Riemann sphere $\mathbb{C} \cup \{\infty\}$.

Proof: In this appendix, we give the sketch of the proof for the main theorem 2.5. See figure 14. In the left frame, a family of planar smooth curves $\Gamma = \{\gamma_0, \cdots, \gamma_5\}$ divide the plane to segments $\{\Omega_0, \Omega_1, \cdots, \Omega_6\}$, where Ω_0 contains the ∞ point. We represent the segments and the curves as a tree in the second frame, where each node represents a segment Ω_k, each link represents a curve γ_i. If Ω_j is included by Ω_i, and Ω_i and Ω_j shares a curve γ_k, then in the tree, the link γ_k connects Ω_j to Ω_i, denoted as $\gamma_k : \Omega_i \to \Omega_j$.

In the third frame, each segment Ω_k is mapped conformally to a circle domain D_k by Φ_k. The signature for each closed curve γ_k is computed $f_{ij} = \Phi_i \circ \Phi_j^{-1}|_{\gamma_k}$, where $\gamma_k : \Omega_i \to \Omega_j$ in the tree.

In the last frame, we construct a Riemann sphere by gluing circle domains D_k's using f_{ij}'s in the following way. The gluing process is bottom up, we first glue the leaf nodes to their fathers. Let $\gamma_k : D_i \to D_j$, D_j is a leaf of the tree. For each point $z = re^{i\theta}$ in D_j, the *extension map*

$$G_{ij}(re^{i\theta}) = re^{f_{ij}(\theta)}.$$

We denote the image of D_j under G_{ij} as S_j. Then we glue S_j with D_i. By repeating this gluing procedure bottom up, we glue all leafs to their fathers. Then we prune all leaves from the tree. Then we glue all the leaves of the new tree, and prune again. By repeating this procedure, eventually, we get a tree with only the root node, then we get a Riemann sphere, denoted as S. Each circle domain D_k is mapped to a segment S_k in the last frame, by a sequence of extension maps. Suppose D_k is a circle domain, a path from the root D_0 to D_k is $\{i_0 = 0, i_1, i_2, \cdots, i_n = k\}$, then the map from $G_k : D_k \to S_k$ is given by

$$G_k = G_{i_0 i_1} \circ G_{i_1 i_2} \circ \cdots \circ G_{i_{n-1} i_n}.$$

Note that, G_0 is identity. Then the Beltrami coefficient of $G_k^{-1} : S_k \to D_k$ can be directly computed, denoted as $\mu_k : S_k \to \mathbb{C}$. The composition $\Phi_k \circ G_k^{-1} : S_k \to \Omega_k$ maps S_k to Ω_k, because Φ_k is conformal, therefore the Beltrami coefficient of $\Phi_k \circ G_k^{-1}$ equals to μ_k.

We want to find a map from the Riemann sphere S to the original Riemann sphere Ω, $\Phi : S \to \Omega$. The Beltrami-coefficient $\mu : S \to \mathbb{C}$ is the union of μ_k's each segments:

$$\mu(z) = \mu_k(z), \forall z \in S_k.$$

By theorem 2.1, the solution exists and unique up to a Möbius transformation. ■

Note that, the discrete computational method is more direct without explicitly solving the Beltrami equation. From the Beltrami coefficient μ, one can deform the conformal structure of S_k to that of Ω_k, under the conformal structures of Ω_k, $\Phi : S \to \Omega$ becomes a conformal mapping. The conformal structure of Ω_k is equivalent to that of D_k, therefore, one can use the conformal structure of D_k directly. In discrete case, the conformal structure is represented as the angle structure 3.1. Therefore in our algorithm, we copy the angle structures of D_k's to S, and compute the conformal map Φ directly.

REFERENCES

[1] Zhu, S.C., Yuille, A.L.: A flexible object recognition and modeling system. IJCV **20** (1996) 8

[2] Liu, T., Geiger, D.: Approximate tree matching and shape similarity. ICCV (1999) 456–462

[3] Belongie, S., Malik, J., Puzicha, J.: Shape matching and object recognition using shape contexts. IEEE Trans. on Pattern Analysis and Machine Intelligence **24** (2002) 509–522

[4] Mokhtarian, F., Mackworth, A.: A therory of multiscale, curvature-based shape representation for planar curves. IEEE Trans. on Pattern Analysis and Machine Intelligence **14** (1992) 789–805

[5] Ericsson, A., Astrom, K.: An affine invariant deformable shape representation for general curves. Proc. IEEE Intl. Conf. on Computer Vision **2** (2003) 1142–1149

[6] Sebastian, T., Klein, P., Kimia, B.: Shock based indexing into large shape databases. European Conf. on Computer Vision **3** (2002) 731–746

[7] Dryden, I., Mardia, K.: Statistical shape analysis. John Wiley and Son (1998)

[8] Yang, Q., Ma, S.: Matching using schwarz integrals. Pattern Recognition **32** (1999) 1039–1047

[9] Lee, S.M., Clark, N.A., Araman, P.A.: A shape representation for planar curves by shape signature harmonic embedding. IEEE Computer Society Conference on Computer Vision and Pattern Recognition (CVPR'06) **2** (2006) 1940–1947

[10] Sharon, E., Mumford, D.: 2d-shape analysis using conformal mapping. International Journal of Computer Vision **70** (2006) 55 – 75

[11] Gardiner, F.P., Lakic, N.: Quasiconformal Teichmller theory. American Mathematical Society (1999)

[12] Henrici, P.: Applied and Computational Complex Analysis. Wiley Classics Library (1974)

[13] R.Munkres, J.: Elements of Algebraic Topology. Addison-Wesley Co. (1984)

[14] Lehto, O., Virtanen, K.: Quasiconformal Mappings in the Plane. Springer-Verlag, New York (1973)

[15] Zeng, W., Zeng, Y., Wang, Y., Yin, X., Gu, X., Samaras, D.: 3D non-rigid surface matching and registration based on holomorphic differentials. In: The 10th European Conference on Computer Vision (ECCV). (2008) 1–14